Impact of grain boundary characteristics on lattice thermal conductivity: A kinetic theory study on ZnO

Xin Liang*

School of Materials Science and Engineering, Changzhou University, Changzhou, Jiangsu 213164, China

(Received 7 February 2017; revised manuscript received 14 March 2017; published 20 April 2017)

Grain boundaries are natural interfaces present in polycrystalline materials and have an important role in transport properties. In this work, the impact of grain boundary crystallographic mismatch, local impurity modulation, and spacing on lattice thermal conductivity is examined from the kinetic theory approach, with ZnO as a case study. We employ a dislocation-based model to describe the grain boundary scatterings of phonons, in which structural characteristics of grain boundaries are explicitly built-in and grain boundary scattering time depends on phonon frequency. This is in contrast to the gray model or the commonly used Casimir limit, which is blind to both grain boundary features and phonon frequency. We show that the lattice thermal conductivity generally decreases with grain boundary misorientation angle, and this dependence is significant for small grain boundary spacing while it tends to diminish for a large one. Intriguingly, our results show that local grain boundary chemistry can affect even more substantially than the crystallographic misfit on phonon relaxation time and interfacial thermal (Kapitza) resistance. Our results suggest new opportunities in tuning lattice thermal conductivity besides the nanostructure engineering approach, and demonstrates the synergetic effects of grain boundary characteristics on phonon conduction in polycrystals.

DOI: 10.1103/PhysRevB.95.155313

I. INTRODUCTION

Understanding the thermal conductivity of materials is one crucial subject in energy and structural materials. For instance, low lattice thermal conductivity is required for both thermoelectrics [1,2] and thermal insulation applications [3,4], whereas materials with excellent heat conduction properties are highly needed for thermal management materials such as in microelectronics [5]. Thermal conductivity consists of lattice (phonon) and electronic contributions. In a large number of materials of interests, the electronic contribution can be ignored as compared to the phonon contribution due to the low electrical conductivity, according to the Wiedemann-Franz law. Lattice thermal conductivity, with phonon as heat carriers, is influenced by multiple phonon scattering processes, including interactions with other phonons (anharmonic scattering) and material defects of various dimensions. Investigations have been successfully carried out on various phonon scattering processes including interactions with other phonons (anharmonic scattering) [6–8], point defects [9,10], dislocations [11,12], interfaces [13–15], and boundaries [16–18] and even nanopores [19]. Recently, the research interests in the role of grain boundaries (GBs) on lattice thermal conductivity, which are naturally existing interfaces in polycrystals, has experienced a renaissance [20,21]. A study on $Si_{1-x}Ge_x$ nanocomposites shows that thermal conductivity is dominated by grain boundaries rather than by alloying [22]. Not only in thermoelectric materials, grain boundary thermal transport also attains research attention in carbon based materials like graphene [23] and diamond [24] for heat sink applications. Notwithstanding these achievements, most of these investigations were based on molecular dynamic simulations and primarily focus on grain size effect.

Grain boundary misorientation angle should have a significant influence on lattice thermal conductivity since propagating phonon waves encounter a change of crystal direction or periodicity across GB. In addition, impurities can segregate at oxide grain boundaries [25] and is expected to create a local mass and strain contrast. The segregation of Pr and Bi elements at ZnO GBs have been verified by atomic resolution transmission electron microscopy (TEM) [26–28] and first-principle calculations [29–31], which accounts for the nonlinear electrical behavior of ZnO [32]. Nevertheless, thermal transport properties of chemically modified ZnO grain boundaries have not yet been investigated.

In this paper, we employ a kinetic theory approach to compute the lattice thermal conductivity of ZnO with various grain boundary characteristics. The inverse phonon lifetime coefficient of anharmonic scattering is obtained in a rigorous way and used for later calculations. We applied a dislocation-based model to describe the grain boundary structure and the associated phonon scattering, in which the GB phonon relaxation time is frequency dependent. Despite the approximations in the complex interactions between phonon scattering and phonon velocity, the present work provides new insights into the role of length scale, crystallographic and chemical characteristics of grain boundaries on phonon conduction. The approach offers a clue to design or modify GB structure for desired phonon transport properties in polycrystalline materials of scientific and technological interests, such as thermoelectrics, thermal barrier coatings, and thermal management materials.

II. DESCRIPTION OF THE MODEL

We begin with the physics of lattice thermal conductivity, which is commonly given by the kinetic theory

$$\kappa = \int_0^\infty \kappa(\omega)\,d\omega = \frac{1}{3}\int_0^\infty C(\omega)v_g(\omega)\Lambda(\omega)\,d\omega = \frac{1}{3}\int_0^\infty C(\omega)v_g(\omega)^2\tau(\omega)\,d\omega, \quad (1)$$

*Corresponding author: liangxin@cczu.edu.cn

where $C(\omega)$ is the volumetric specific heat capacity, $v_g(\omega)$ is the group velocity of phonons, Λ is the phonon mean free path (MFP), and $\tau(\omega)$ is the phonon relaxation or scattering time, also known as phonon lifetime. Yang and Dames [33] reformed the equation by changing the integration variable from ω to Λ as

$$\kappa = \int_0^\infty \kappa_\Lambda(\omega)\, d\Lambda = -\frac{1}{3}\int_0^\infty C(\omega) v_g(\omega)\Lambda(\omega)\left(\frac{d\Lambda}{d\omega}\right)^{-1} d\Lambda. \quad (2)$$

The above transformation provides a more intuitive physical picture. Interatomic spacing generally sets the lower bound for phonon MFP [34], and we choose the minimum MFP $\Lambda_{\min}$ as a half of the c-axis lattice parameter of ZnO unit cell which is 2.6 Å. Since $\Lambda(\omega)$ is normally a monotonically decreasing function of ω, the minimum MFP $\Lambda_{\min}$ gives a upper limit of integral $\omega_{\max}$ in Eq. (1). We take this back to a mathematically convenient form of Eq. (1), which is given by [8,9],

$$\kappa = \frac{k_B}{2\pi^2 v_s}\left(\frac{k_B T}{\hbar}\right)^3 \int_0^{x_{\lim}} \tau(x)\frac{x^4 e^x}{(e^x-1)^2} dx, \quad (3)$$

with $x = \hbar\omega/k_B T$ a dimensionless parameter as the integration variable, and the upper limit of integral $x_{\lim} = \hbar\omega_{\max}/k_B T$. The phonon relaxation time $\tau(x)$ is determined from the individual scattering process via Matthiessen's rule

$$\tau(x)^{-1} = \sum_i \tau_i(x)^{-1} = \tau_U^{-1} + \tau_D^{-1} + \tau_B^{-1}, \quad (4)$$

where anharmonic scattering (τ_U), point defect or alloy scattering (τ_D) and grain boundary or interface scattering (τ_B) are most commonly considered.

Above the Debye temperature, the phonon relaxation time associated with anharmonic scattering τ_U relates to the phonon frequency by $\tau_U^{-1} = S(T)\omega^2$, where $S(T) \cong CT$ [9,16,35]. The temperature-independent parameter C is an inverse phonon lifetime coefficient for anharmonic scattering. The C value is mostly obtained by fitting the experimental data [15,21]; however, experimental room temperature thermal conductivity of pure ZnO varies drastically, ranging from 36 to 135 $\mathrm{Wm^{-1}K^{-1}}$ [15,36–40]. Various factors can account for this large variation, such as microstructure and point defects. It is therefore necessary to derive the C value from high-quality single-crystal data. Considering there is nonnegligible anisotropy in phonon conduction along the a and c axes of ZnO, the mean or effective value should be used. The mean thermal conductivity κ_{mean} represents the phonon conduction averaged over crystal orientations, or equivalently, the thermal conductivity of a polycrystal that consists of randomly oriented grains but without the effect of grain boundary scatterings. It can be obtained using a "correlational approximation" model [15,41,42]

$$\frac{\kappa_{\mathrm{mean}}}{\kappa_a} = \frac{r+2}{3} - \frac{2}{9}\frac{(r-1)^2}{r+2}, \quad (5)$$

where $r = \kappa_c/\kappa_a$ is the anisotropy factor, and κ_a and κ_c are lattice thermal conductivity along the a and c axes of the ZnO single crystal, respectively. The measured RT (room temperature) thermal conductivity along the c axis of single-crystal ZnO is about 95−116 $\mathrm{Wm^{-1}K^{-1}}$ [38,40]. A recent density functional theory calculation work on ZnO [43] reports that the lattice thermal conductivity along the a and c axes values are 63 and 95 $\mathrm{Wm^{-1}K^{-1}}$, respectively, with the latter one in good agreement with experiments. Since the measured a-axis value is yet not available, we take the DFT-calculated values for both the a and c axes back to Eq. (5) and obtain $\kappa_{\mathrm{mean}} = 72.64\ \mathrm{W\ m^{-1}\ K^{-1}}$. In putting this value back to Eqs. (3) and (4), the inverse phonon lifetime coefficient for anharmonic scattering in ZnO is obtained as $C = 1.62\times10^{-18}$ s/K, which is on the same order of magnitude as the previously found one [44].

For point defect or alloy scattering, we use the common form [21,45,46], a Rayleigh-like expression $\tau_D^{-1} = V_0\Gamma\omega^4/(4\pi v_g^3)$, where V_0 is the volume per atom. $\Gamma = \sum_i f_i(1-m_i/\bar{m})^2$ relates to the mass disorder where f_i and m_i are the fraction and the atomic mass of defect species i, respectively, and $\bar{m}$ is the average mass of all atoms. For simple materials like ZnO, we use the Debye model so that the phonon group velocity v_g and phase velocity v_p can be approximated as the constant of sound velocity v_s [35], which is given in terms of the longitudinal v_L and transverse v_T wave velocities $3/v_s^3 = 1/v_L^3 + 2/v_T^3$. In putting $v_L = 6365$ m/s and $v_T = 2735$ m/s for bulk ZnO [37], we obtain $v_g \approx v_s = 3090$ m/s.

The general form of phonon relaxation time due to grain boundary scattering is $\tau_B^{-1} = v_g/Fd$ [47,48], where d is the GB spacing. F relates to the specularity of the boundary scattering and is not clearly known. $F = 1$ is commonly taken so that the equation reduces to the Casimir limit $\tau_B^{-1} = v_g/d$, which represents a rough boundary surface and purely diffusive scattering [49]. Apparently, the Casimir model (also known as the gray model) describes the boundary scattering as phonon frequency-independent, with an implication that the boundary scattering strength of phonons is a constant and unaffected by GB characteristics except the spacing. In this work, we treat grain boundary as described by an array of dislocations; for symmetric tilt grain boundary, the dislocation spacing at GB, D, relates to the GB misorientation angle θ according to [50]

$$\frac{1}{D} = \frac{2\sin\theta/2}{b}, \quad (6)$$

where b is the Burgers vector. Equation (6) shows that the linear dislocation density along GB, $1/D$, increases with crystallographic mismatch. Accordingly, the phonon lifetime associated with GB scattering can be described based on phonon scattering by arrays of dislocations [16,45], which consists of phonon scattering time due to dislocation cores τ_{DC} and strain field τ_{DS}

$$\tau_{DC}^{-1} = N_D\frac{V_0^{4/3}}{v_g^2}\omega^3, \quad (7)$$

$$\tau_{DS}^{-1} = 0.6 b_{\mathrm{eff}}^2 N_D(\gamma+\gamma')^2 \times\left\{\frac{1}{2}+\frac{1}{24}\left(\frac{1-2r}{1-r}\right)^2\left[1+\sqrt{2}\left(\frac{v_L}{v_T}\right)^2\right]^2\right\}, \quad (8)$$

where $N_D \approx 2/(d\times D)$ is the converted areal dislocation density. b_{eff} is the magnitude of effective Burgers vector and

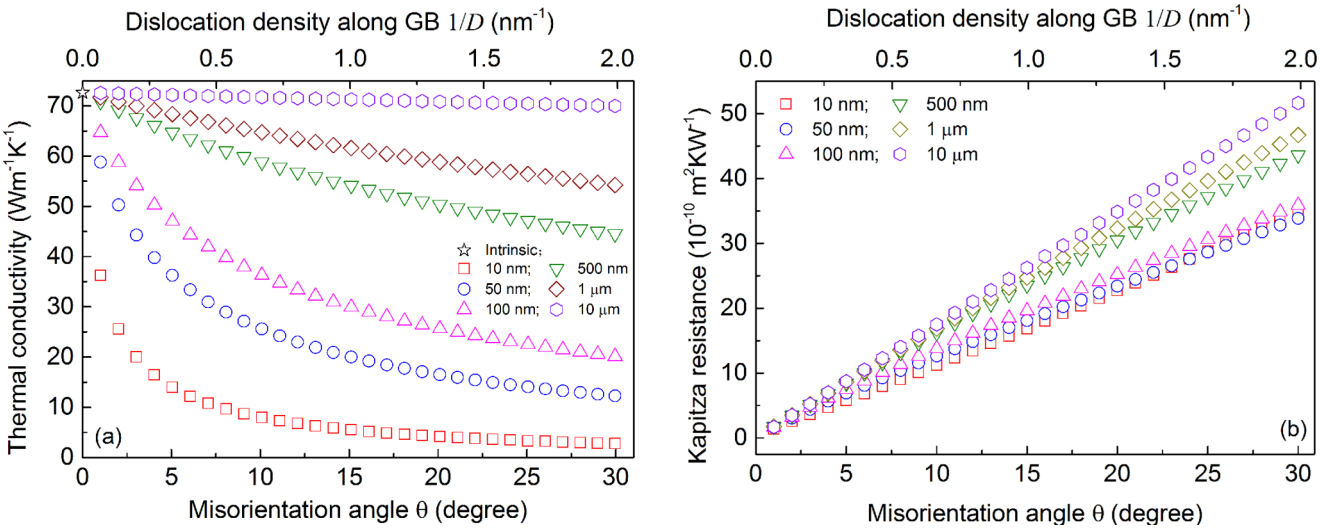

FIG. 1. (a) Calculated room temperature ZnO thermal conductivity and (b) the derived grain boundary Kapitza resistance as a function of grain boundary misorientation angle for grain boundary spacing ranging from 10 nm to 10 μm. The corresponding linear dislocation density along grain boundary is indicated on the top axis. The intrinsic thermal conductivity of ZnO is also superimposed on the figure.

can be approximated to be lattice parameter. r is the Poisson's ratio and is 0.337 for bulk ZnO [51]. γ is the Grüneisen parameter, and it has an approximated value of 0.75 for tetrahedrally bonded structure. γ' is the change in Grüneisen parameter due to impurity modulation and is given by [52]

$$\gamma' = \frac{V_0 c K}{k_B T_a}(\gamma\alpha^2 - \alpha\beta), \tag{9}$$

where c is the impurity segregation concentration. $K = E/3(1-2r)$ is the bulk modulus and can be obtained from Young's modulus E and Poisson's ratio r. T_a is the annealing temperature at which the material is last thermally equilibrated and a common value of 1273 K is used. α and β are the atomic volumetric difference and mass mismatch, respectively, which are given as

$$\alpha = \frac{V_i - V_0}{V_0}, \quad \beta = \frac{1}{2}\frac{m_0 - m_i}{m_0}, \tag{10}$$

where the subscript 0 and i refers to the host and impurity species, respectively. With Eqs. (6) to (10), the impact of grain boundary characteristics on lattice thermal conductivity, including misorientation angle, local chemical modulation, and spacing, can be evaluated.

III. RESULTS AND DISCUSSIONS

In Fig. 1(a), we present RT thermal conductivity of ZnO with grain boundary misorientation angle up to 30°, or equivalently the corresponding linear dislocation density along GB, for a range of GB spacing from 10 nm to 10 μm. Seen from the plot, thermal conductivity decreases with increasing crystallographic misfit or defect density at GB, which is significant for small GB spacing d because a large fraction of phonons encounter GB scatterings. In addition, thermal conductivity for small GB spacing drops quickly at low misorientation angle θ and saturates to a constant that is basically unchanged with further increase in θ. In contrast, thermal conductivity is less affected by θ for large grain size, in which the GB spacing is generally much larger than the phonon MFP. For instance, for $d = 10\,\mu$m, there is only a slight reduction in thermal conductivity when θ increases from 0 to 30°. Assuming thermal resistance in series, the Kapitza resistance R_k can be readily derived from the equation

$$\frac{1}{\kappa} = \frac{1}{\kappa_i} + \frac{R_k}{d}, \tag{11}$$

where κ is the effective thermal conductivity of polycrystalline ZnO, κ_i is the intrinsic one and d is the grain boundary spacing. The Kapitza resistance of ZnO grain boundaries versus GB misorientation angle is plotted in Fig. 1(b). Notably, irrespective of grain boundary spacing, the Kapitza resistance R_k increases with θ, from a few to tens of 10^{-10} m^{2}K/W. This range covers well the measured values 13, 45, and 49.8×10^{-10} m^{2}K/W for grain boundaries of Si [53], YSZ [54], and $SrTiO_3$ [55]. By comparing Figs. 1(a) and 1(b), one sees the synergetic effect of GB spacing and crystallographic mismatch on lattice thermal conductivity. For instance, for $d = 10\,\mu$m, although there is a considerable increase in R_k with increasing θ, the lattice thermal conductivity is virtually unchanged.

We now examine the influence of grain boundary impurity segregation on phonon conduction. Although Pr and Bi have very low solid solubility in ZnO lattice, generally smaller than 0.5 mol.% [56,57], the occupancy of Pr and Bi atoms on Zn^{2+} sites can be quite high at GBs. For instance, first-principle calculations suggests that Bi concentration can be up to 12.5 mol.% at ZnO $\sum = 13$ grain boundary [29]; structure unit analysis based on atomic resolution electron microscopy suggests that Pr concentration segregated at ZnO GB can be as high as 15 mol.% [26]. We use these values as the limit of ZnO GB impurity segregation concentration for our calculations. We chose the grain boundary spacing of 500 nm and a misorientation angle of 15° for computing the thermal conductivity. Shown in Fig. 2(a), the thermal conductivity decreases with increasing impurity segregation concentration. Bi segregation is found to have a more significant effect than Pr in reducing the thermal conductivity. This is attributed

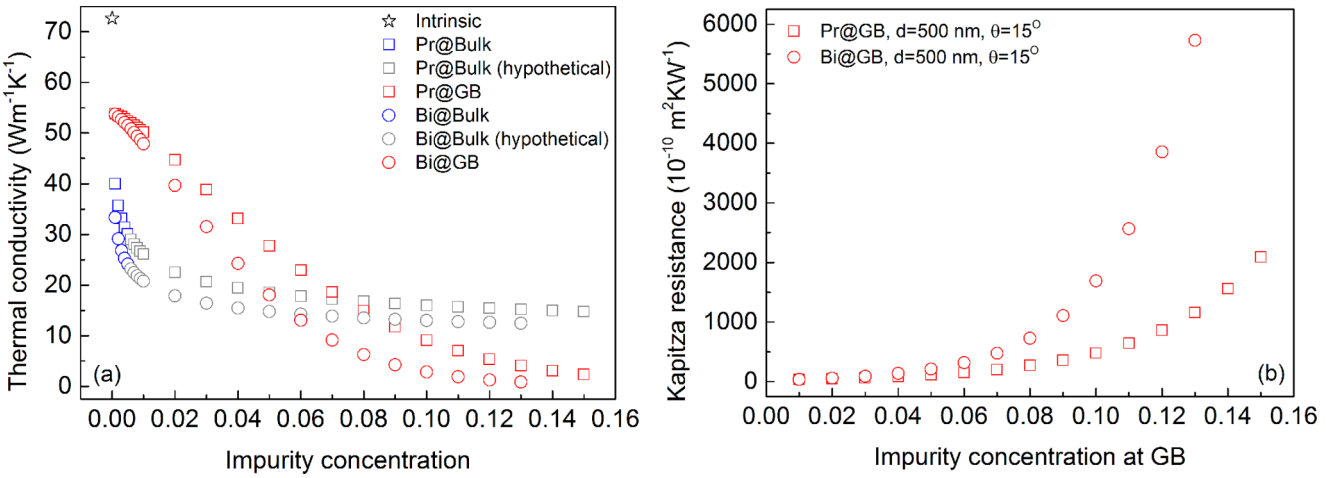

FIG. 2. (a) Calculated room temperature ZnO thermal conductivity as a function of impurity concentration for Pr (open square) and Bi (open circle) elements, respectively. The thermal conductivity data consist of two sets: the ZnO with all impurity atoms segregate on GBs (red symbols) and ZnO solid solutions with "clean" GBs (blue symbols). To show the contrast between the effects of point defect and GB impurity segregation on phonon scattering, hypothetical ZnO solid solutions with impurity concentration beyond the solid solubility limit is also presented (gray symbols). All calculations are performed on a GB spacing of 500 nm with a misorientation angle of 15°. (b) Derived Kapitza resistance as a function of impurity segregation concentration at ZnO GBs.

to the relatively large atomic volumetric mismatch and mass difference at GB created by Bi atoms, which can be seen by comparing the values of α and β using Eq. (10). To make a comparison to the point-defect-dominated phonon scattering, we calculate the thermal conductivity of ZnO solid solutions in which all impurity species substituting Zn^{2+} sites in bulk while leaving "clean" grain boundaries of the same spacing. Both Pr and Bi have the valency of +3 and create substitutional defects $M_{Zn}^{\bullet}$ (M = Pr, Bi) and cationic vacancies $V_{Zn}^{''}$ for site and charge balance [27–29]. Due to the intrinsically low solid solubility of Pr and Bi in ZnO bulk, impurity concentration beyond 0.005 is considered as hypothetical solid solutions. Interestingly, with increasing impurity concentration, there is a cross-over between the thermal conductivity of ZnO with impurities at GBs and ZnO solid solutions, for both Pr and Bi. Our results imply that by local impurity modulation, grain boundary scattering can further bring down the lattice thermal conductivity when point defect scattering becomes almost ineffective. In Fig. 2(b), we show the Kapitza resistance as a function of GB impurity segregation concentration. For the same impurity segregation concentration, Bi-modified GB has a larger value of R_k than Pr. The most striking feature in Fig. 2(b) is the dramatic increase in R_k when GB impurity segregation concentration goes above ~0.06. The room temperature R_k reaches 2089 and 5726×10^{-10} m^{2}K/W for of [Pr] = 0.15 and [Bi] = 0.13, respectively. To make a comparison, the highest reported value of room temperature R_k is about $\sim1200\times10^{-10}$ m^{2}K/W which is measured from the interface of Bi/hydrogen-terminated diamond [58]. Our calculation results can, to some extent, overestimate the grain boundary impurity segregation effect, while keeping in mind that most of the reported R_k values are measured from "clean" interfaces. Theoretically, there is no upper limit for R_k, and as high as about $30\,000\times10^{-10}$ m^{2}K/W has been reported for the Al-3Si/diamond interface at 50 K [20].

The influence of grain boundary characteristics on phonon scatterings is better understood from the analysis of the phonon relaxation time against frequency. Seen from Fig. 3(a), the phonon lifetime due to GB scattering based on the Casimir model is frequency-independent, which is commonly seen in the literature [35,59]. In contrast, the dislocation-based GB scattering model suggests a strong frequency dependence of phonon populations, especially at low frequencies. The phonon relaxation time decreases with increasing GB misorientation angle, implying the enhanced phonon scattering with crystallographic mismatch. Local chemical modulation at GB by Pr and Bi further reduces the phonon lifetime by several orders of magnitude. The frequency dependence of the phonon contribution to lattice thermal conductivity can be seen from the spectral thermal conductivity κ_s [16,35]

$$\kappa_s = \frac{3k_B\omega^2}{2\pi^2 v_g}\tau(\omega). \tag{12}$$

Apparently, grain boundary primarily scatter low- to mid-frequency (or equivalently, mid- to long-wavelength) phonons, as shown in Fig. 3(b). For anharmonic scattering, the spectral thermal conductivity is invariant with phonon frequency since the ω^2 term in Eq. (12) is cancelled out by ω^{-2} in τ_U. Interestingly, the dislocation-based GB model shows a narrower frequency "window" of strong phonon scattering than the Casimir model. For a certain frequency, the phonon lifetime and spectral thermal conductivity can vary by orders of magnitude due to the change in GB misorientation angle and impurity segregation, whereas the commonly used Casimir model is unseeing to these factors.

Finally, we examine the role of grain boundary spacing, which intuitively affects the phonon MFP. We perform the analysis based on MFP spectrum and thermal conductivity accumulation function approach, which is a powerful way of quantifying the phonon mode contributions to the thermal conductivity [33,46,60–62]. Assuming the isotropic bulk dispersion relations and MFP, we first calculate the cumulative thermal conductivity $\kappa_{\rm cum} = \int_{\Lambda_{\rm min}}^{\Lambda_\alpha} \kappa_\Lambda(\omega) d\Lambda$, which gives

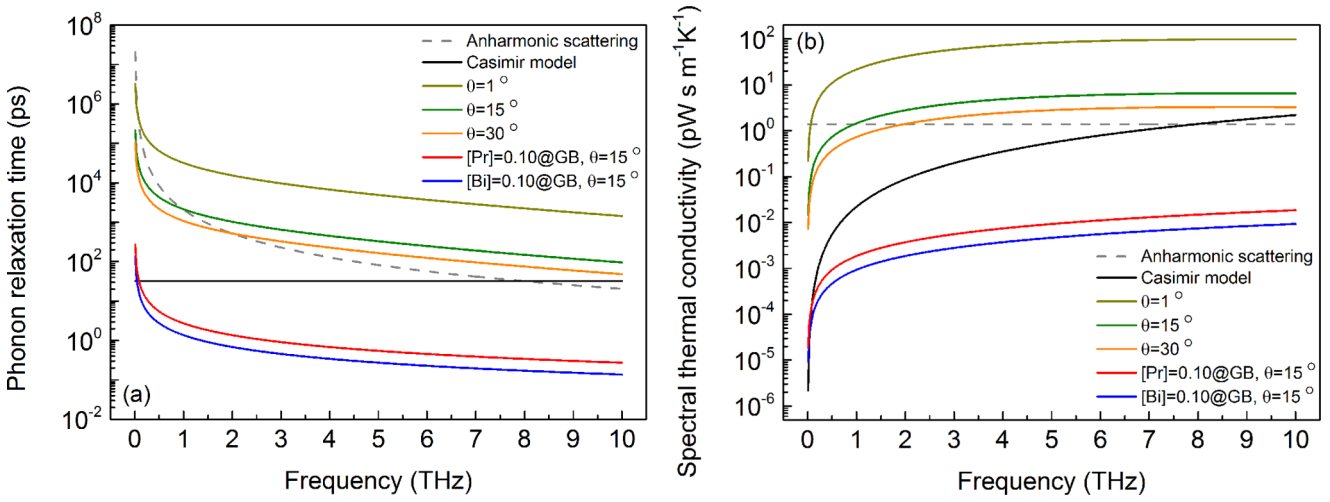

FIG. 3. (a) Frequency dependence of phonon relaxation time and (b) spectral thermal conductivity for ZnO with various grain boundary characteristics: "clean" GBs with misorientation angle of 1, 15, and 30° and [Pr] = [Bi] = 0.10 segregated GBs with misorientation angle of 15°. Calculations are performed for room temperature and grain size of 100 nm. Also shown are the Casimir model and anharmonic scattering for comparison.

the absolute contribution value to the thermal conductivity provided by the phonon modes up to Λ_α. In Fig. 4(a), we show the cumulative thermal conductivity as a function of phonon MFP for grain boundary spacing ranging from 5 nm to 10 μm for the same misorientation angle of 15°. The intrinsic curve is calculated based on anharmonic scattering and shown as reference to reveal the role of grain boundary spacing in reducing the thermal conductivity. Apparently, nanoscale grain boundary spacing leads to tremendous reduction in thermal conductivity, whereas for large grain boundary spacing like 10 μm the MFP distribution is almost indistinguishably close to the intrinsic one. The thermal conductivity accumulation function is then readily obtained, $\alpha = \int_{\Lambda_{\min}}^{\Lambda_\alpha} \kappa_\Lambda(\omega) d\Lambda / \int_{\Lambda_{\min}}^{\infty} \kappa_\Lambda(\omega) d\Lambda$, which is the normalized value characterizing the fractional contribution. Interestingly, the corresponding thermal conductivity accumulation function curves appear similar, as shown in Fig. 4(b), and the large GB spacing curve ($d = 10\,\mu$m) virtually overlaps with the intrinsic one. Close observation reveals that as d decreases, the contribution from short MFP phonon modes becomes smaller and the phonon MFP distribution appears sharper. Furthermore, the thermal conductivity accumulation function of small GB spacing quickly asymptote towards the bulk value, whereas the accumulation function of intrinsic and large GB spacing has a longer tail in the large phonon MFP regime. For instances, the thermal conductivity accumulation function for $d = 5$ nm reaches the bulk value roughly at MFP of 300 nm whereas the intrinsic one still has apparent contributions from longer MFP phonons.

The remarkable influence of GB characteristics on lattice thermal conductivity, as predicted by the kinetic theory approach, is expected to raise fundamental interests in materials science and suggests a new avenue of experimental work. For instance, by careful design and growth of ZnO bicrystals, the

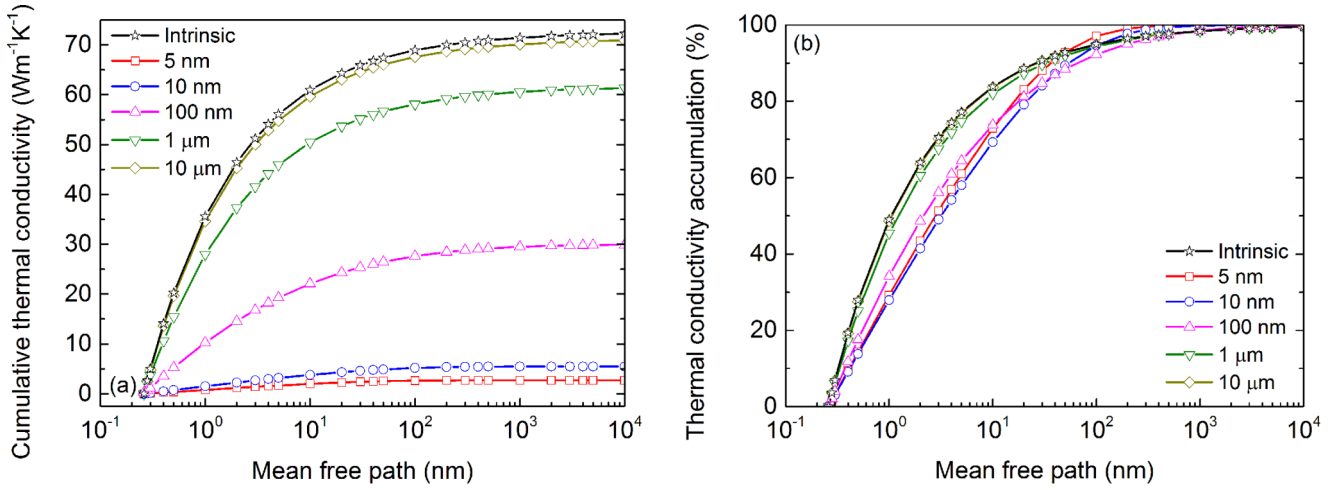

FIG. 4. (a) Cumulative thermal conductivity and (b) thermal conductivity accumulation function versus phonon MFP for different grain boundary spacing. All GBs are impurity-free and have a misorientation angle of 15°. Anharmonic scattering is considered in all calculations. Also shown is the intrinsic behavior where phonon conduction is solely governed by anharmonic scattering.

misorientation angle of grain boundaries can be controlled and determined; the bicrystal GB can also be enriched with alien elements using a diffusion couple approach. Then, direct measurement of the thermal conductance across the bicrystal GB can provide the experimental results. The effect of grain boundary spacing can be seen on samples of a wide range of grain sizes, which can be made by nanomaterials synthesis, advanced sintering and postannealing.

IV. CONCLUSIONS

In conclusion, we present a kinetic theory approach and predict that grain boundary crystallographic mismatch, chemical modulation, and spacing have a remarkable impact on lattice thermal conductivity, demonstrated on ZnO. We show that these factors in concert change the grain boundary Kapitza resistance and consequently the lattice thermal conductivity, with impurity modulation offering an unexpectedly large reduction in boundary conductance. Besides the commonly used nanostructure engineering where spacing is the frequently used control factor, we suggests new possibilities for engineering the lattice thermal conductivity via modifying the grain boundary crystallography and chemistry. Our results can have important implications for applications such as thermoelectrics, thermal insulation, and heat dissipation.

ACKNOWLEDGMENTS

This work was supported by National Natural Science Foundation of China (Grant No. 51502024), Distinguished Professorship of Jiangsu Province, and Jiangsu Six Talent Summit Plan (No. 2015XCL037).

[1] L. D. Zhao, S. H. Lo, Y. S. Zhang, H. Sun, G. J. Tan, C. Uher, C. Wolverton, V. P. Dravid, and M. G. Kanatzidis, Nature (London) **508**, 373 (2014).
[2] G. J. Snyder and E. S. Toberer, Nat. Mater. **7**, 105 (2008).
[3] D. R. Clarke, Surf. Coatings Technol. **163-164**, 67 (2003).
[4] N. P. Padture, M. Gell, and E. H. Jordan, Science **296**, 280 (2002).
[5] A. A. Balandin, Nat. Mater. **10**, 569 (2011).
[6] P. G. Klemens, *Theory of the Thermal Conductivity of Solids* (Academic Press, New York, 1968).
[7] M. G. Holland, Phys. Rev. **132**, 2461 (1963).
[8] J. Callaway, Phys. Rev. **113**, 1046 (1959).
[9] J. Callaway and H. C. von Baeyer, Phys. Rev. **120**, 1149 (1960).
[10] C. Wan, Z. Qu, Y. He, D. Luan, and W. Pan, Phys. Rev. Lett. **101**, 085901 (2008).
[11] Y. Ni, S. Xiong, S. Volz, and T. Dumitrică, Phys. Rev. Lett. **113**, 124301 (2014).
[12] D. Kotchetkov, J. Zou, A. A. Balandin, D. I. Florescu, and F. H. Pollak, Appl. Phys. Lett. **79**, 4316 (2001).
[13] C.-W. Nan and R. Birringer, Phys. Rev. B **57**, 8264 (1998).
[14] M. N. Luckyanova *et al.*, Science **338**, 936 (2012).
[15] X. Liang, M. Baram, and D. R. Clarke, Appl. Phys. Lett. **102**, 223903 (2013).
[16] H.-S. Kim, S. D. Kang, Y. Tang, R. Hanus, and G. J. Snyder, Mater. Horizons **3**, 234 (2016).
[17] M. Omini and A. Sparavigna, Phys. Rev. B **61**, 6677 (2000).
[18] K. P. Tai, A. Lawrence, M. P. Harmer, and S. J. Dillon, Appl. Phys. Lett. **102**, 034101 (2013).
[19] C. Bera, N. Mingo, and S. Volz, Phys. Rev. Lett. **104**, 115502 (2010).
[20] C. Monachon, L. Weber, and C. Dames, Annu. Rev. Mater. Res. **46**, 433 (2016).
[21] Z. Wang, J. E. Alaniz, W. Jang, J. E. Garay, and C. Dames, Nano Lett. **11**, 2206 (2011).
[22] C. Melis and L. Colombo, Phys. Rev. Lett. **112**, 065901 (2014).
[23] A. Cao and J. Qu, J. Appl. Phys. **111**, 053529 (2012).
[24] D. Spiteri, J. Anaya, and M. Kuball, J. Appl. Phys. **119**, 085102 (2016).
[25] B. Feng, T. Yokoi, A. Kumamoto, M. Yoshiya, Y. Ikuhara, and N. Shibata, Nat. Commun. **7**, 11079 (2016).
[26] J. Y. Roh, Y. Sato, and Y. Ikuhara, J. Am. Ceram. Soc. **98**, 1932 (2015).
[27] Y. Sato, T. Mizoguchi, N. Shibata, T. Yamamoto, T. Hirayama, and Y. Ikuhara, Phys. Rev. B **80**, 094114 (2009).
[28] Y. Sato, J. P. Buban, T. Mizoguchi, N. Shibata, M. Yodogawa, T. Yamamoto, and Y. Ikuhara, Phys. Rev. Lett. **97**, 106802 (2006).
[29] J. M. Carlsson, H. S. Domingos, P. D. Bristowe, and B. Hellsing, Phys. Rev. Lett. **91**, 165506 (2003).
[30] W. Korner and C. Elsasser, Phys. Rev. B **81**, 085324 (2010).
[31] W. Korner, P. D. Bristowe, and C. Elsasser, Phys. Rev. B **84**, 045305 (2011).
[32] D. R. Clarke, J. Am. Ceram. Soc. **82**, 485 (1999).
[33] F. Yang and C. Dames, Phys. Rev. B **87**, 035437 (2013).
[34] G. Grimvall, *Thermalphysical Properties of Materials* (North-Holland, Amsterdam, 1999).
[35] E. S. Toberer, A. Zevalkink, and G. J. Snyder, J. Mater. Chem. **21**, 15843 (2011).
[36] T. Olorunyolemi, A. Birnboim, Y. Carmel, O. C. Wilson, I. K. Lloyd, S. Smith, and R. Campbell, J. Am. Ceram. Soc. **85**, 1249 (2002).
[37] J. Alvarez-Quintana, E. Martinez, E. Perez-Tijerina, S. A. Perez-Garcia, and J. Rodriguez-Viejo, J. Appl. Phys. **107**, 063713 (2010).
[38] D. I. Florescu, L. G. Mourokh, F. H. Pollak, D. C. Look, G. Cantwell, and X. Li, J. Appl. Phys. **91**, 890 (2002).
[39] X. Liang and D. R. Clarke, Acta Mater. **63**, 191 (2014).
[40] U. Ozgur *et al.*, J. Electron. Mater. **35**, 550 (2006).
[41] E. A. Mityushov, R. A. Adamesku, and P. V. Gel'd, J. Eng. Phys. **47**, 1052 (1984).
[42] F. Yang, T. Ikeda, G. J. Snyder, and C. Dames, J. Appl. Phys. **108**, 034310 (2010).
[43] A. Consiglio and Z. T. Tian, Sci. Rep. **6**, 36875 (2016).
[44] X. Liang, Ph.D. thesis, Harvard University, 2013.
[45] P. G. Klemens, Proc. Phys. Soc. London Sect. A **68**, 1113 (1955).
[46] J. Garg, N. Bonini, B. Kozinsky, and N. Marzari, Phys. Rev. Lett. **106**, 045901 (2011).
[47] N. Mingo, Phys. Rev. B **68**, 113308 (2003).

[48] N. Mingo, L. Yang, D. Li, and A. Majumdar, Nano Lett. **3**, 1713 (2003).
[49] E. S. Toberer, L. L. Baranowski, and C. Dames, Annu. Rev. Mater. Res. **42**, 179 (2012).
[50] A. Kelly, G. W. Groves, and P. Kidd, *Crystallography and Crystal Defects*, rev. ed. (John Wiley & Sons, Chichester, England, 2000).
[51] C. Qin, Y. Gu, X. Sun, X. Wang, and Y. Zhang, Nano Res. **8**, 2073 (2015).
[52] A. J. Friedman, Phys. Rev. B **7**, 663 (1973).
[53] D. G. Cahill, M. Katiyar, and J. R. Abelson, Phys. Rev. B **50**, 6077 (1994).
[54] A. M. Limarga and D. R. Clarke, Appl. Phys. Lett. **98**, 211906 (2011).
[55] Y. F. Wang, K. Fujinami, R. Z. Zhang, C. L. Wan, N. Wang, Y. S. Ba, and K. Koumoto, Appl. Phys. Express **3**, 031101 (2010).
[56] S. Y. Chun, N. Wakiya, H. Funakubo, K. Shinozaki, and N. Mizutani, J. Am. Ceram. Soc. **80**, 995 (1997).
[57] J. R. Lee, Y. M. Chiang, and G. Ceder, Acta Mater. **45**, 1247 (1997).
[58] H. K. Lyeo and D. G. Cahill, Phys. Rev. B **73**, 144301 (2006).
[59] R. Cheaito, J. C. Duda, T. E. Beechem, K. Hattar, J. F. Ihlefeld, D. L. Medlin, M. A. Rodriguez, M. J. Campion, E. S. Piekos, and P. E. Hopkins, Phys. Rev. Lett. **109**, 195901 (2012).
[60] A. J. Minnich, Phys. Rev. Lett. **109**, 205901 (2012).
[61] T. Hori, J. Shiomi, and C. Dames, Appl. Phys. Lett. **106**, 171901 (2015).
[62] K. T. Regner, D. P. Sellan, Z. Su, C. H. Amon, A. J. H. McGaughey, and J. A. Malen, Nat. Commun. **4**, 1640 (2013).